DOI: https://doi.org/10.46354/i3m.2019.iwish.004

A MULTI-MODAL DATA MODEL FOR MORPHOLOGICAL SEGMENTATION IN 3D DOSIMETRY

Werner Backfrieder

Dept. Biomedical Informatics, University of Applied Sciences Upper Austria, Hagenberg, Austria

Werner.Backfrieder@fh-hagenberg.at

ABSTRACT

Patient specific dosimetry established during the last decade in modern radio-therapy. Usually, tracer kinetics in main compartments of observed metabolism is assessed from anterior and posterior whole body scans. The effective doses for each organ, derived by the MIRD scheme, provide evidence for following radio-therapeutic treatment and helps to meet vital dose limits for critical organs, e.g. kidneys. The calculation of individual dose in a three-dimensional context leads to more accurate dose estimates, as was proven by intensive research, but is still on the cusp to clinical application.

In this work, a statistical approach, based on multi-modal image and feature data, is presented, to overcome manual segmentation, the most time consuming step, in 3D based dose calculation. 3D data volumes from a hybrid SPECT study, comprising SPECT and CT data, covering main compartments of metabolism, build the image features of a Gaussian classifier. From prior segmentations organ-specific membership maps are derived, and substituted as additional feature into the segmentation procedure. Centroids, eccentricity and principal axes of organ models are registered to a rough thresholded image of the SPECT component, and define membership coefficients of the voxels.

The new approach yields accurate results, even with real patient data. The new method needs minimal user interaction during selection of some sample regions, thus showing high potential for implementation in a clinical workflow.

Keywords: medical internal dosimetry, image registration, segmentation

1. INTRODUCTION

Radiotherapy is a strongly evolving branch in modern nuclear medicine. In contrast to tele-therapy, it affects the lethal impact, by transfer of the radioactive particles directly into the tumour. Accumulation processes in the tumour-tissue, utilizing specific bindings of trace-molecules, shall reduce the region of lethal effects to the target region and protect surrounding tissues, specifically essential organs, from radiation stress.

Nuclear medicine therapy came always along with radiation protection. First attempts were made using static phantoms, built from bottles (Bush 1949), yielding rough dose estimates, for each radiopharmaceutical and therapy application under consideration.

Consideration of patient scans leads to individual dose planning. Exposure data, measured from organ scans, are combined with Monte-Carlo dose calculations, based on standardized phantom geometries. Standardized tabulated values exist for each therapeutic isotope, applied to various different human models, e.g. pediatric, female, pregnant, and male body phantoms. Results for all relevant body compartments are published in the ICRP reports. The principles are implemented in the software package MIRDOSE (Stabin 1996), the clinical standard until 2004, before OLINDA was deployed (Stabin and Siegel 2003).

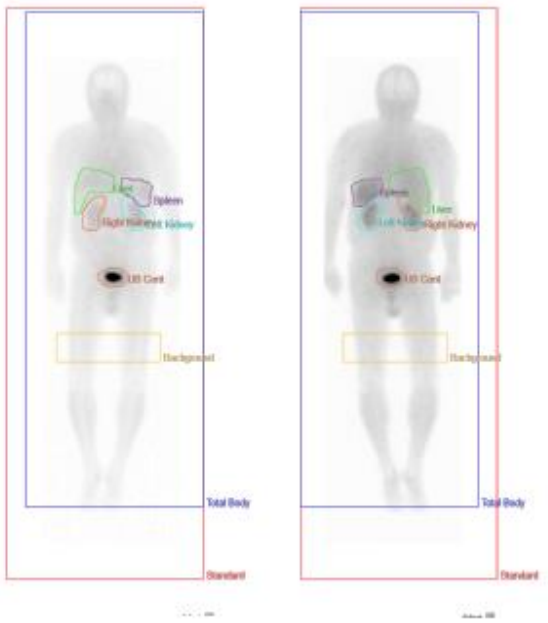

Figure 1: Manually drawn regions used for dose calculation. Regions are drawn over whole body scans, displayed in anterior and posterior view: kidneys (brown, cyan), liver (green), spleen (purple), bladder (ocher), body background (gold), total body (blue), and the reference standard (orange).

With the further development of imaging modalities, anthropomorphic models are refined towards realistically shaped organs. These models are derived from segmentation of measured 3D data (Schläger 2011).

Individual dose planning focuses on the assessment of pharmacokinetics and accumulation of the radioactive isotope in every single patient. Most therapeutic radiopharmaceuticals are mainly beta emitters and have

no or only weak gamma lines in their emission spectra, inhibiting assessment of radioactive uptake. In this case an isotope with similar pharmacokinetics but strong gamma spectrum is substituted to perform the dose estimation scans. Time activity curves for all relevant organs, providing the essential information for the following dose calculation, are estimated from emitted cumulative counts. Regions of interest (ROIs) are drawn manually over the whole body images and evaluated at each point in time, cf. Fig1. To correct for the latter applied therapeutic isotope the summed counts are modified, reflecting the physical half-life-time of the therapeutic isotope (Mirzarei et al 2013).

Projection may lead to overlapping ROIs in 2D scans making accurate rating of concerned TACs very difficult. Approaches with factor analysis were made for distinguishing overlapping regions, utilizing small differences in tracer dynamics (Backfrieder et al. 1996, Backfrieder and Zwettler 2015, Sámal et al. 1987, 1989)

Recent approaches of individual dose planning are based on hybrid tomography data, SPECT-CT or PET-CT, in combination with 2D whole body data series for estimation of temporal evolution dose distribution (Lee 2015, Backfrieder 2018), but until now costly image acquisition and data processing in 3D are drawbacks in clinical application of 3D dosimetry.

In the current approach a method for automated segmentation in 3D based on bi-modal SPECT-CT Data is developed, substituting a statistical membership map as further feature to a standard Gaussian discrimination process to improve segmentation, thus fostering 3D dosimetry in clinical procedures.

2. MATERIALS

Imaging protocol for dose estimation in nuclear medicine radiation therapy comprises multiple patient studies. A three dimensional SPECT scan, together with a low dose CT scan, provide general information about specific uptake in a 3D context, and the CT allows attenuation correction for further improvement estimating true source counts. Temporal behavior is derived from a series of planar whole body images.

Data from six patients, three male and three female, age ranging from 52 to 79 years, are examined. Each patient study comprises a SPECT and CT volume image, and six planar whole body scans.

2.1. Whole body scans

After administration of 60 MBq In-111, whole body scans are acquired 20 min, 90 min, 24h, 48h, 72h, and 96h after injection. Image data are acquired with a double-headed gamma camera, Philips BrightView. Detectors are in 180 degree position. Anterior and posterior data are captured on a 1024x512 image matrix, 2.8mm pixel-size and scan-speed 10cm/min. Figure 2 shows the full whole body series in anterior view.

Images are scaled to individual data ranges. In early images, the content of the urinary bladder dominates the image dynamics, thus diminishing organ contrast. In latter frames, kidneys show higher relative intensity indicating the washing out of radioisotopes from blood. Uptake of liver and spleen is increasing; urinary bladder shows still substantial filling. The following frames show main residence of the radioactive substances in liver, spleen and kidneys. The residence times in spleen and liver are slightly higher than in kidneys, indicated by higher count rates. Accumulation in these organs is responsible for main dose stress.

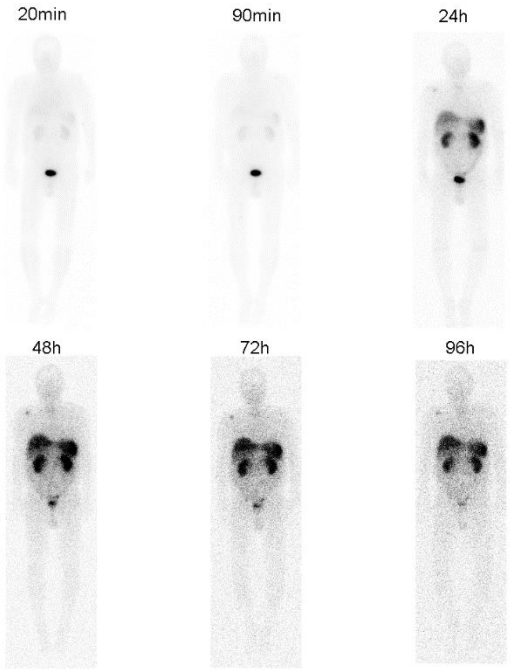

Figure 2: Anterior projection data set. The series of whole body scans shows the dynamic processes, six scans cover a period of 96 hours. Projection images are acquired on a 1024 by 512 matrix, with 10cm/min scan speed. The intensity window is scaled to 45% of the maximum in each individual frame.

2.2. Volume scans

SPECT and CT data are taken directly after the 90 min planar whole body scan. SPECT projections are acquired on an elliptical, body approaching orbit with 3 degrees rotational increment, 20s acquisition time on a 130x130 matrix, with a squared FOV of 605mm length. A series consists of 90 slices, with thickness 4.66mm. Images are reconstructed with an OSEM algorithm and attenuation corrected. CT data are on a 512x512 matrix with isotropic voxel-size of 1mm. The volume comprises 406 slices. Figure 3 shows an identical slice from both SPECT (a) and CT (b).

3. METHODS

The MIRD approach leads to an estimate of effective doses for each organ, respectively compartment, considering it as mutual source and target for all others (Snyder et al. 1975). To obtain realistic dose values, estimates need reliable measurements of emitted radiation. In standard clinical procedures, regions are manually drawn over the whole body scans and accumulated counts build the samples for the time

activity curves (TACs), yielding the total counts over this region. However, this approach suffers from general information loss in 2D projection images. For proper consideration of attenuation effects and correction of overlapping regions, three-dimensional segmentation is inevitable. Manual segmentation by drawing regions slice by slice is very time consuming and besides scientific case studies, it is not likely to take place in a clinical workflow.

Global thresholding of the SPECT image volumes is not sufficient, since organs aggregating radiation touch each other, e.g. liver and kidney, or liver and spleen, and no sufficient discrimination is achievable. Manual post-processing needs roughly the same efforts as manual segmentation.

A full data set for preparation of radio-therapy comprises, besides the planar whole body studies, a SPECT and a CT volume scan, as described in the materials section. The mutual information from SPECT and CT is the basis for segmentation, since CT images comprise detailed morphological information. Both volumes build a multivariate data model, each pixel has a SPECT and CT feature value. Gaussian discrimination is intended to obtain accurate segmentation. CT data are actually acquired for attenuation correction, hence weak x-ray intensity keeps additional patient dose low, but causes low contrast in image data. The reduced contrast resolution is not sufficient for accurate differentiation between considered tissues. As a further dimension, a membership feature is substituted, representing a flexible model build from former segmentations.

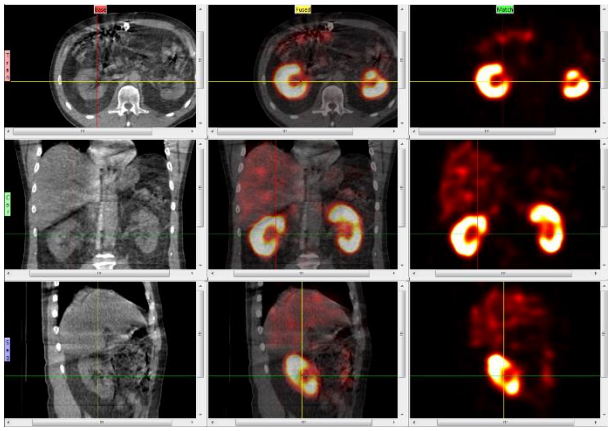

Figure 3: Co-Registration of CT and SPECT image volumes. Primary registration inherent to the hybrid camera (Philips BrightView) is further refined by MI voxel based registration. Columns show CT, CT-SPECT overlay, and SPECT images in transversal, coronal, and sagittal slice orientation.

3.1. Thresholding

Segmentation is a workflow comprising many steps. During the first step, scan data are prepared for segmentation. Double thresholds are applied to the CT and the SPECT image volumes to exclude all voxels, outside the limits, from further consideration. All the segmented voxels are subject to multispectral classification. In this process, voxels with similar features are grouped together. The features are its respective intensity value in the specific modalities and the value from the probability map, defining a fuzzy membership to a tissue type. Exact registration of the scans is an inevitable requirement for successful registration.

3.2. Registration

Mutual information is a statistical measure from information theory; it describes the relation of symbols in two coherent data sets, respective tissues or morphologies. It is extensively used in image registration of multimodal data, where correlation methods are not applicable to modality specific manifestation of tissue. In perfectly registered images, mutual information is maximized (Studholme et al. 1996, Hill et al. 1998, Crum et al. 2003).

For aligment of two-dimensional images, X and Y, the global maximum in a three-dimensional variable space, one rotational and two translational degrees of freedom, is determined. Mutual information of both images is maximized by steepest gradient search

$$MI(X;Y) = \sum_{y \in Y} \sum_{x \in X} p(x,y) \log\left(\frac{p(x,y)}{p(x)\,p(y)} \right). \qquad (1)$$

In the above equation $p(x,y)$ denotes the joint probability of images X and Y, the probabilities of both single images are represented by $p(x)$ and $p(y)$.

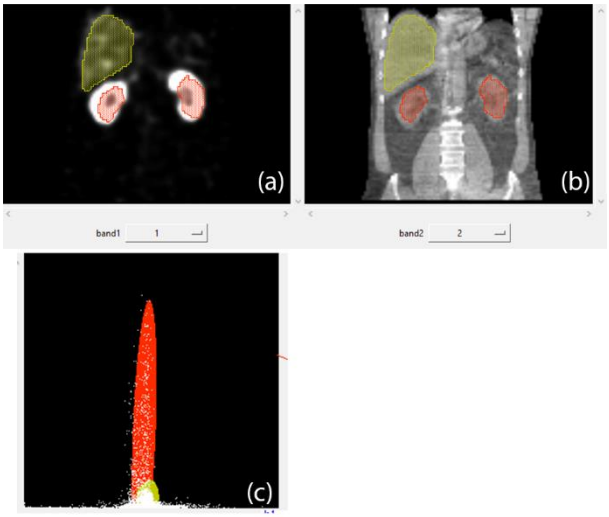

Figure 4: Feature images with samples for liver (green-yellow) and kidneys (red). Regions for sampling are drawn simultaneously on, both the SPECT image (a) and CT image (b). The distributions derived from the samples are drawn over the scattergram (c).

3.3. Multi-spectral classification

Co-registered data build the base features of the multispectral classification procedure. Intensity values of a specific tissue type or organ, in respective modality, build clusters in feature space, i.e. the scattergram. Each voxel is an object in feature space, and its position is determined by the intensity values along the axes. In this work we us a simple Gaussian data model for clustering

(Kaufman and Rousseeuw 2005). But the approach can easily refined by substituting another clustering technique.

In this model, each tissue type is described by a multivariate Gaussian distribution.

$$f(\vec{x}) = \frac{1}{\sqrt{(2\pi)^p \|\Sigma\|}} \exp\left(-\frac{1}{2}(\vec{x}-\vec{\mu})^T \Sigma^{-1}(\vec{x}-\vec{\mu})\right) \quad (2)$$

The $\vec{x}$ is the object or voxel with the image values from each modality and the rest of the *p* features describing the object-characteristics, $\vec{\mu}$ is the mean of the distribution, and Σ the covariance matrix.

For first estimates for the parameters $\vec{\mu}$ and Σ, regions are drawn manually over the tissues, and the estimates are calculated, based on these. Figure 4 shows an example for these regions. Regions are displayed over the feature images, too. The application allows choice of any feature as image slice in two canvases. The regions are displayed in different colors, selected voxels are colored in the scatergram, displayed at the bottom. After selecting samples the first estimate of the distributions are calculated. The distributions are limited by an α value, to achieve optimal segmentation. In the example shown in Figure 4.c a value of 0.03 is chosen.
These initial distributions are the starting points for an iterative procedure to refine segmentation. The distributions are used for segmentation of the whole image volume in each step. The intermediate segmentations are the samples for the next iteration, providing new estimates for mean and covariance and updated distributions for the next iteration. In this approach, a fixed number of 5 iterations is applied.

3.4. Topological membership map

A topological membership map is built to further support segmentation, since SPECT and CT values provide sometimes weak differentiation between tissue types. The map is based on prior segmentations. Relevant features as centroids, principal axes, eccentricity and some statistical moments are estimated from these data sets. Each new segmentation updates this parameter, leading to a steadily improving prior model. The model is globally registered against the preliminary segmentation after thresholding, to provide an initial position. The single organs are further adapted to local shape of the given segment. For each organ, a topological map is substituted as artificial feature to the multispectral classifier.

4. RESULTS

As a proof of concept for the elaborated segmentation method, anonymized clinical data from patient studies are processed. Topological membership maps provide useful information to employ Gaussian clustering for meaningful automated segmentation. Segmentation of liver and kidney based solely on SPECT and CT data is shown in Figure 6.a. Samples are drawn, as shown in Figure 4.a and 4.b, on representative slices, of the coronary cut. Regions are drawn on the adjacent slices, also, to reach sufficient sample size. The distributions calculated by classification on a confidence interval of 97% are displayed over the scattergram, cf. to the bottom row of Figure 4.c. The resulting classification is shown in Figure 6.a. Identified soft tissue voxels are colored, liver is shown as green-yellow and kidneys are labeled red. To keep comparability in Figure 6 the same slice is displayed as in Figure 4. As clearly seen, clustering based on CT and SPECT data, without any position information, provides very poor segmentation. Most of the classifications are wrong. The method, without any further improvement, is not applicable for segmentation, as shown in Figure 6.a.

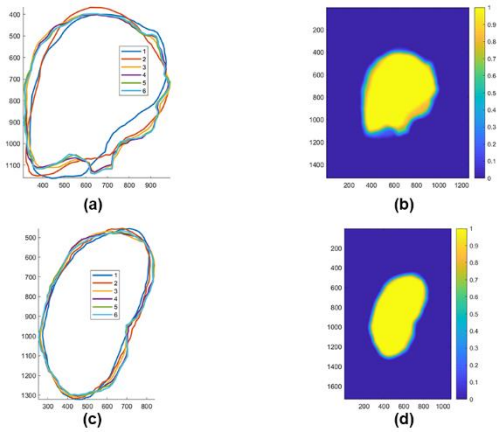

Figure 5: Standardized topological membership maps generated from most significant PCs. Topological models are calculated for liver (top row) and kidney (bottom row). Figures (a) and (c) show the cumulative contours from PC1 up to PC 6. The maps in (b) and (d) show the probability maps for membership based on these PC-curves.

Topological membership maps substitute the required position information. A principal component model of a priori known outer contours gathered from former segmentations is built. The contours are registered to each other and resampled on an equally spaced angular grid, to provide point correspondence for PCs. The resulting PC models are shown in Figure 5 on the left column. The curve of the first, most significant PC represents the average shape of all captured contours. All further contours represent the deviations from the prior curves. The plot shows the curves for liver and right kidney reconstructed from 1 up to 6 components, cf. Figure 5.a and 5.c. These curves are converted to probabilities by accumulation of the regions surrounded by the PC curves. Figure 5.b and 5.d display the maps for liver and right kidney. Substitution of topological membership maps provides the additional position information to achieve proper segmentation. Figure 6.b shows the improved results. Kidneys are clearly visible and accurately distinguished from surrounding tissue. Liver is slightly over-segmented, but superior to the segmentation before. Post-processing with morphological operations may further improve results. The proposed method of topological membership maps is self-learning. Each new segmentation is added to the

data pool, providing new variability and diversity of contours. By the way, the PC model is further refined.

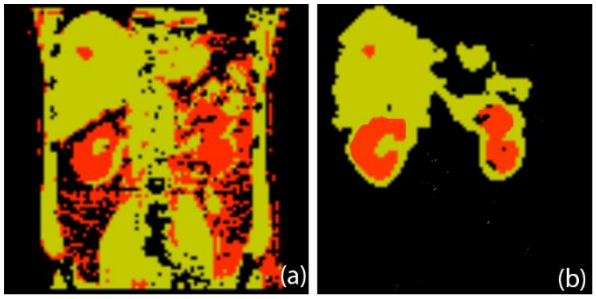

Figure 6: Automated segmentation based on multispectral classification. Liver (green-yellow) and kidneys (red) are classified. (a) Classification based on SPECT counts and CT units, solely, yield weak results. Substitution of topological membership maps improves segmentation substantially (b).

5. DISCUSSION

Internal dosimetry raises its importance with the increasing availability of a great variety of tracer molecules, enabling individual tumor therapy. Ethic and legal constraints put focus on reliable and accurate dosimetry. With common whole body scintigraphy, problems of overlapping organs in projections and deterioration of counts by attenuation are inherent to the method. The installation of modern 3D imaging modalities allow a three dimensional sight of the problem, at the cost of at least two additional scans and some very time consuming data processing. This work proposes a reasonable approach for mainly automated definition of 3D VOIs with little user interaction collecting representative sample data, in contrast to manual drawing organ ROIs.

The method is promising for establishing 3D dosimetry as standard in clinical daily routine, but it still needs improvement by further post processing and careful testing with clinical data.

REFERENCES

Backfrieder W, Baumgartner R, Sámal M, Moser E, Bergmann H, 1996. Quantification of intensity variations in functional MR images using rotated principal components. *Phys Med Biol.* 1996, 41(8), 1425-38.

Backfrieder W, Zwettler G, 2015. Rotated Principal Components for fuzzy segmentation of szintigraphic time series in individual dose planning. Proceedings of the 4th International Workshop on Innovative Simulation for Healthcare, 2015, Bergeggi, Italy, 2015: 6-12

Backfrieder W, 2018. An approach for attenuation corrected 3D internal radiation dosimetry. Proceedings of the 7th International Workshop on Innovative Simulation for Health Care, 2018, Budapest, Hungary, Hungary, 2018: 38-42

Bush F, 1949. The integral dose received from a uniformly distributed radioactive isotope. British J Radiol. 22:96-102.

Crum WR, Hill DL, Hawkes DJ, Information theoretic similarity measures in non-rigid registration. *Inf Process Med Imaging*. 2003 Jul, 18, 378-87.

Hill DL, Maurer CR , Jr, Studholme C, Fitzpatrick JM, Hawkes DJ, 1998. Correcting scaling errors in tomographic images using a nine degree of freedom registration algorithm. *J Comput Assist Tomogr*. 1998 Mar-Apr, 22(2), 317-23.

Mirzaei S, Sohlberg A, Knoll P, Zakavi R, Diemling M, 2013. Easy-to-use online software package for internal dose assessment after radionuclide treatment in clinical routine. *Clin Nucl Med*. 2013, 38(9), 686-90.

Kaufman L, Rousseeuw P, 2005. Finding groups in data. Wiley & Sons, Inc., Hoboken, New Jersey.

Lee JA, Ahn YC, Lim DH, Park HC, Asranbaeva MS, 2015. Dosimetric and clinical influence of 3D versus 2D planning in postoperative radiation therapy for gastric cancer. *Cancer Res Treat*. 2015 Oct, 47(4),727-37.

Sámal M, Kárný M, Sůrová H, Maríková E, Dienstbier Z, 1987. Rotation to simple structure in factor analysis of dynamic radionuclide studies. *Phys Med Biol.* 1987, 32(3), 371-82.

Sámal M, Kárný M, Sůrová H, Pěnicka P, Maríková E, Dienstbier Z, 1989. On the existence of an unambiguous solution in factor analysis of dynamic studies. *Phys Med Biol*. 1989, 34(2), 223-8.

Schläger M, 2011. Comparison of various anthropomorphic phantom types for in vivo measurements by means of Monte Carlo simulations. *Radiat Prot Dosimetry*, 2011 Mar, 144(1-4),384-8.

Snyder WS, Ford MR, Warner GG, Watson SB, 1975. "S," Absorbed dose per unit cumulated activity for selected radionuclides and organs. Oak Ridge National Laboratory, Oak Ridge, Tennessee, USA

Stabin JA, 1996. MIRDOSE: personal computer software for internal dose assessment in nuclear medicine. *J Nucl. Med.* 1996, 37(3), 538-46.

Stabin JA, Siegel MG, 2003. Physical models and dose factors for use in internal dose assessment. *Health Physics*, 2003 Sep, 85(3), 294-310.

Studholme C, Hill DL, Hawkes DJ, 1996. Automated 3-D registration of MR and CT images of the head. *Med Image Anal.* 1996 Jun, 1(2), 163-75.

AUTHORS BIOGRAPHY

Werner Backfrieder received his degree in technical physics at the Vienna University of Technology in 1992. Then he was with the Department of Biomedical Engineering and Physics of the Medical University of Vienna, where he reached a tenure position in 2002. Since 2002 he is with the University of Applied Sciences Upper Austria at the division of Biomedical Informatics. His research focus is on Medical Physics and Medical Image Processing in Nuclear Medicine and Radiology with emphasis to high performance computing. Recently research efforts are laid on virtual reality techniques in the context of surgical planning and navigation.